



Non-classical correlations of accelerated observers interacting with a classical stochastic noise beyond the single mode approximation

M. Y. Abd-Rabbou¹ · M. Shamirzaie² · Salman Khan³

Received: 6 April 2023 / Accepted: 6 May 2023 / Published online: 9 June 2023
© The Author(s) 2023

Abstract

This paper investigates the behaviour of the quantum correlations for an accelerated two-qubit system during its interaction with a classical stochastic field, utilizing the Wigner function and concurrence. The non-classical behaviour is indicated by negative values of the Wigner function, while the degree of entanglement is demonstrated by the concurrence. To consider acceleration and interaction with a common or independent environment, we discard the single-mode approximation and utilize the Unruh construction of the quantum field mode in our analysis. Our results suggest that coherence suppression is caused by the acceleration effect, noise strength, and noise frequency. Through an examination of quantum concurrence, this study analyses the level of quantum entanglement that corresponds positively with negative values of the Wigner function. The findings indicate that coherence degradation in the initial system is reduced when observers interact independently with their environments, as opposed to interacting with a common environment. Additionally, the acceleration of both observers has an impact on coherence reduction. During system evolution, the Wigner function displays collapse and reappearance behaviour, while quantum entanglement undergoes local collapse and revival phenomena. Notably, common noise situations exhibit more rapid variation in both the Wigner function and entanglement compared to independent noise configurations.

Keywords Wigner function · Entanglement · Accelerated systems · Stochastic noise

✉ M. Y. Abd-Rabbou
m.elmalky@azhar.edu.eg

M. Shamirzaie
mshj@iaush.ac.ir

Salman Khan
sksafi@comsats.edu.pk

¹ Mathematics Department, Faculty of Science, Al-Azhar University, Nasr City, Cairo 11884, Egypt

² Department of Physics, Islamic Azad University, Shahreza, Isfahan 311-86145, Iran

³ Department of Physics, COMSATS Institute of Information Technology, Park Road, Islamabad 45550, Pakistan

1 Introduction

The relation between the quasi-probability distributions and quantum correlations remains a significant issue in quantum information theory (Ferrie 2011; McConnell et al. 2015; Arkhipov et al. 2018). Numerous studies have shown that probabilistic quasi-distributions represent a composite measure, in which their positive values represent the classical correlations, whereas the negative values indicate the quantum correlations (Abd-Rabbou et al. 2019; Franco and Penna 2006). These distribution functions are widely used in the computation of quantum correlations within the classical dynamics of a nano-mechanical resonator (Mohamed and Metwally 2018). It also may be used to illuminate the quantum density state within the visualization of phase space (Miquel et al. 2002). In fact, there are three discrete quasi-probabilistic functions that are reconstructed in s -parametrized form: Husimi Q -function (Husimi 1940), Wigner function (Wigner et al. 1997; Chumakov and Klimov 2002) and Glauber-Sudarshan P -function (Sudarshan 1963), with $s = -1, 0, 1$ respectively. What is more, there are different constructions of quasi-probability in accordance with the phase space, such as the radiation field (Moya-Cessa and Knight 1993), the $SU(2)$ angular momentum basis via atomic coherent states (Agarwal 1981; Klimov et al. 2017), the $SU(3)$ Lie algebra (Rowe et al. 1999), and $SU(1,1)$ (Seyfarth et al. 2020). Of particular significance are the negative values of the Wigner function, which not only depict the entanglement and decoherence of the quantum system, but also play an integral role in quantum state tomography (López and Paz 2003; Dahl et al. 2006; Paz et al. 2004).

The Wigner function has been used to investigate the $2N \times 2N$ discrete phase space of N orthogonal quantum systems, as demonstrated in Gibbons et al. (2004). For different quantum systems, the Wigner function has been widely discussed, including superconducting flux qubits (Reboiro et al. 2015), the accelerated two-qubit state in the presence of noise channels (Abd-Rabbou et al. 2019), tripartite W -state (Abd-Rabbou et al. 2020), GHZ state (Metwally et al. 2019), two non-equivalent resonators (Abgaryan et al. 2021), and a cavity coupled to atomic system (Mavrogordatos 2021). In addition, using Wigner distribution as a measure of quantum correlation for tripartite GHZ and W states have been studied experimentally (Ciampini et al. 2022).

From the perspective of physicists, quantum regimes are highly susceptible to interaction and environmental influence. Therefore, the impact of different environments on quantum correlations has garnered the attention of scientists. Studies have been conducted on the effect of acceleration processes on the entanglement of two-qubit and qubit-qutrit systems (Tian et al. 2012; Metwally 2017, 2019). Additionally, the influence of dephasing noisy environments on the information of two-qubit states has been examined (Yu and Eberly 2003; Karlsson et al. 2016). Recently, various classical noise channels have become an important factor in influencing quantum systems as they approach real-world scenarios (Lo and Chau 1999; Smith et al. 2011). The dynamics of quantum coherence, quantum correlation, and the degree of estimation in the presence of a classical coloured noise channel have been investigated (Khan and Shamirzaie 2020; Metwally and Ebrahim 2020). The quantum skew information and quantum coherence of an accelerated two-qubit system with random telegraph noise have been studied (Abd-Rabbou et al. 2022). The dynamics of entanglement, coherence, and mixedness of a tripartite quantum state have been analysed under power-law and random telegraph noises (Rahman et al. 2022).

In this paper, our aim is to investigate how the Wigner function can indicate entanglement in both Markovian and non-Markovian environments for an accelerated two-qubit system. To achieve this, we will not rely on the single mode approximation and instead

transform the Minkowski quantum field modes into the Rindler ones. We will model the effect of the environment using classical random telegraph noise, which can be applied to qubits independently or commonly. As is well known, a density operator’s non-separability is characterized by negative elements in its Wigner function. This negativity can serve as an indicator of entanglement in a two-qubit system. The paper is structured as follows: Sect. 2 presents the physical model of the quantum system and reviews essential tools for accelerating systems. In Sect. 3, we introduce analytical forms of the quasi-probability distributions, namely the Wigner function and quantum concurrence. Section 4 is dedicated to constructing density operators in various scenarios. In Sect. 5, we provide explicit forms of the Wigner function and concurrence as measures of quantum entanglement for the mentioned density operators. We investigate their behaviours for accelerated systems and highlight the effects of noise, acceleration, and discarding the single-mode approximation. Finally, in Sect. 6, we summarize our results.

2 Quantum correlation measures

In this section, we will provide a mathematical review of the concurrence and negative values of the Wigner function, which may serve as a suitable measure of quantum correlations. Let us consider a density operator $\hat{\rho}_{AB}$ with an X -structure. In the computational basis $\{|00\rangle, |01\rangle, |10\rangle, |11\rangle\}$, $\hat{\rho}_{AB}$ can be expressed as follows,

$$\hat{\rho}_{AB} = \rho_{11}|00\rangle\langle 00| + \rho_{22}|01\rangle\langle 01| + \rho_{33}|10\rangle\langle 10| + \rho_{44}|11\rangle\langle 11| + (\rho_{14}|00\rangle\langle 11| + \rho_{23}|01\rangle\langle 10| + H.C.), \tag{1}$$

where ρ_{ij} are corresponding components in the computational basis.

2.1 Concurrence

As it is widely recognized, the entanglement produced between two particles, denoted as A and B , can be conveniently quantified by means of concurrence. Specifically, the concurrence for the X -structure of a density operator $\hat{\rho}_{AB}$ is defined as follows (Hill and Wootters 1997),

$$\mathcal{C} = \max[0, |\rho_{14}| - \sqrt{\rho_{22}\rho_{33}}, |\rho_{23}| - \sqrt{\rho_{11}\rho_{44}}]. \tag{2}$$

The function \mathcal{C} is constrained to the interval $[0, 0.5]$. When $\mathcal{C} = 0$, the density operator $\hat{\rho}_{AB}$ is completely separable, whereas it attains maximum entanglement at $\mathcal{C} = 0.5$.

2.2 Wigner function

To capture non-classical correlations that go beyond entanglement, we will utilize the negative values of the Wigner function. Also, constructing the atomic Wigner probability distribution in $Su(2)$ algebra for a two-qubit system can be provided valuable insights into the nature of non-classical correlations beyond entanglement. For a two-qubit system, the atomic Wigner distribution can be defined as (Agarwal 1981),

$$\mathcal{W}_\rho(\theta, \phi) = 2\pi \operatorname{Tr} \left[\hat{\rho}_{AB} \left(\bigotimes_{i \in \{a,b\}} \left(\hat{L}_{0,0}^{(i)} \mathbf{Y}_{0,0}^{(i)}(\theta, \phi) + \sum_{n=-1}^1 \hat{L}_{1,n}^{(i)} \mathbf{Y}_{1,n}^{(i)}(\theta, \phi) \right) \right) \right], \quad (3)$$

here $\mathbf{Y}_{l,m}^i(\theta, \phi)$ are the spherical harmonics functions, and $\hat{L}_{L,m}^{(i)}$ are the orthogonal irreducible tensor operators in $\frac{1}{2}$ -spin representation are given by:

$$\hat{L}_{L,m}^{\dagger(i)} = (-1)^m \sqrt{\frac{2L+1}{2}} \sum_{i,i'=-\frac{1}{2}}^{\frac{1}{2}} C_{\frac{1}{2}, i, L, -m}^{\frac{1}{2}, i'} \left| \frac{1}{2}, i' \right\rangle \left\langle \frac{1}{2}, i \right|$$

where $C_{\frac{1}{2}, i, L, -m}^{\frac{1}{2}, i'}$ are the Clebsch-Gordon coefficients. Here $\hat{L}_{L,m}^{(i)}$ for our case can be calculated as:

$$\begin{aligned} \hat{L}_{0,0}^i &= \frac{1}{\sqrt{2}} (|0\rangle_i \langle 0| + |1\rangle_i \langle 1|), & \hat{L}_{1,0}^i &= \frac{-1}{\sqrt{2}} (|0\rangle_i \langle 0| - |1\rangle_i \langle 1|), \\ \hat{L}_{1,-1}^i &= |1\rangle_i \langle 0| = -\hat{L}_{1,1}^{i\dagger} \end{aligned}$$

After some straightforward calculation, one can get the Wigner function for the X -state (6) in $\frac{1}{2}$ -spin representation as,

$$\begin{aligned} \mathcal{W}_\rho(\theta, \phi) &= 2\pi \left[\rho_{11} A_{11}^2 + (\rho_{22} + \rho_{33}) A_{11} A_{00} + \rho_{44} A_{00}^2 \right. \\ &\quad \left. + (\rho_{23} A_{01} A_{10} + \rho_{14} A_{01}^2 + H.C.) \right]. \end{aligned} \quad (4)$$

where the functions A_{ij} are defined by the following spherical harmonics,

$$\begin{aligned} A_{11} &= \frac{1}{\sqrt{2}} (\mathbf{Y}_{0,0}(\theta, \phi) - \mathbf{Y}_{1,0}(\theta, \phi)), & A_{01} &= -\mathbf{Y}_{1,1}(\theta, \phi), \\ A_{10} &= \mathbf{Y}_{1,-1}(\theta, \phi), & A_{00} &= \frac{1}{\sqrt{2}} (\mathbf{Y}_{0,0}(\theta, \phi) + \mathbf{Y}_{1,0}(\theta, \phi)). \end{aligned}$$

Via substituting the spherical harmonics with their values in eq. (4), and take the negative values of the Wigner function, one can obtain the atomic Wigner function of X -structure as,

$$\begin{aligned} \mathcal{W}_\rho(\theta, \phi, t) &= \min \left\{ 0, \frac{1}{4} \left[1 + 2\sqrt{3} \cos \theta (\rho_{11} - \rho_{44}) + 3 \cos^2 \theta (\rho_{11} - \rho_{22} - \rho_{33} + \rho_{44}) \right. \right. \\ &\quad \left. \left. + 6 \sin^2 \theta (\rho_{23} + \rho_{14} \cos 2\phi) \right] \right\}. \end{aligned} \quad (5)$$

For a two-qubit system, the function $\mathcal{W}_\rho(\theta, \phi, t) \in [-0.5, 0)$, where $\mathcal{W}_\rho(\theta, \phi, t) = -0.5$ represents a maximally quantum correlation.

3 The basis formalism and the physical models

In this section, we present the fundamental formalism for studying the dynamics of quantum correlations between two observers, Alice and Bob, whose qubits are being subjected to interactions with their respective environments while one or both of them undergo uniform acceleration relative to an inertial coordinate system. We assume that each observer possesses a qubit and that their collective quantum state is initially prepared in a mixed state ($t = 0$ and prior to any quantum information task) with a density matrix of the following form,

$$\rho_{AB}(0) = x|\psi\rangle_{AB}\langle\psi| + \frac{(1-x)}{4}\mathbb{1}, \tag{6}$$

where A, B refer to Alice and Bob, respectively, $|\psi\rangle_{AB} = \frac{1}{\sqrt{2}}(|00\rangle + |11\rangle)$, $\mathbb{1}$ is identity matrix on a four dimensional Hilbert space and $x \in [0, 1]$ is a measure for the purity of the state. Moreover, we ascribe 0's and 1's as the occupation of a fermionic quantum field, with specific energy E and momentum P . As outlined in the Introduction, our objective is to examine classical and quantum correlations among accelerating observers. Therefore, we assume that Bob and/or Alice uniformly accelerate with respect to an inertial observer after sharing the qubits. To investigate scenarios where some observers accelerate, quantization in non-inertial frames becomes necessary. Essentially, this involves quantizing the quantum field in non-inertial frames. It is widely recognized that an observer in a non-inertial frame with constant proper acceleration a perceives the vacuum state of the field as a thermal distribution of field quanta, which is known as the Unruh effect (Unruh 1976). This phenomenon has been extensively studied in the literature. The world line of an observer moving with constant proper acceleration is a two-fold hyperbolic curve, as illustrated in Figure 1 of reference (Bruschi et al. 2010). These hyperbolas are distinct and causally disconnected, located in two separate regions known as the right and left Rindler wedges. The right hyperbolic curve corresponds to the worldline of a real observer, while the left one corresponds to that of a fictitious observer. For accelerating observers, the appropriate basis for quantizing field modes is the Rindler basis (Takagi 1986), rather than the Minkowski or Unruh basis used by inertial observers. If the (anti)particle operators for Minkowski, Rindler and Unruh basis are (a_i^M, b_i^M) , (a_i^Σ, b_i^Σ) and (A_i^R, B_i^R) , respectively, where $\Sigma = I, II$ are two wedges of Rindler coordinates and $\mathcal{R} = R, L$ are two independent basis for Unruh modes, then these modes are related by Bogoliubov transformations as (Bruschi et al. 2010; Takagi 1986):

$$a_i^M = \int_0^\infty (\alpha_{ik}^{I*} a_k^I + \beta_{ik}^I b_k^{I\dagger} + \alpha_{ik}^{II*} a_k^{II} + \beta_{ik}^{II} a_k^{II\dagger}) dk \tag{7}$$

$$A_i^R = \cos r a_i^I + \sin r b_i^{II\dagger} \tag{8}$$

$$A_i^L = \cos r a_i^{II} - \sin r b_i^{I\dagger}. \tag{9}$$

Here α_{ik}^Σ and β_{ik}^Σ are the Bogoliubov coefficients, and the parameter r is related to the acceleration, a through $\tan r = e^{-\pi\omega c/a}$ where ω is the mode frequency which accelerating observer measures and c is the speed of light. The Unruh one particle creation operator is a combination of two contribution of Left and Right Unruh operators:

$$A_i^{U\dagger} = R A_i^{R\dagger} + L A_i^{L\dagger} \tag{10}$$

In Eq. (10), R and L are complex numbers satisfying the condition $|R|^2 + |L|^2 = 1$. By suitably localized Minkowski modes one can get the desired narrow peak of Unruh modes which are themselves related to single modes of Rindler basis. This setting just corresponds to $R = 1$ (and hence $L = 0$), and is known as single mode approximation (SMA).

The Bogoliubov transformations between filed operators enable us to express the vacuum $|0_k\rangle_{\mathcal{M}}^+$ and the first excited state $|1_k\rangle_{\mathcal{M}}^+$ of the Dirac filed in Minkowski basis for a specific k -mode in terms of Rindler basis. These transformations are:

$$\begin{aligned} |0_k\rangle_{\mathcal{M}}^+ &= \cos^2 r |0_k\rangle_I^+ |0_{-k}\rangle_{II}^- |0_k\rangle_{II}^+ - \sin r \cos r |0_k\rangle_I^+ |0_{-k}\rangle_{II}^- |1_{-k}\rangle_{II}^- |1_k\rangle_{II}^+ \\ &\quad + \sin r \cos r |1_k\rangle_I^+ |1_{-k}\rangle_{II}^- |0_{-k}\rangle_{II}^- |0_k\rangle_{II}^+ - \sin^2 r |1_k\rangle_I^+ |1_{-k}\rangle_{II}^- |1_{-k}\rangle_{II}^- |1_k\rangle_{II}^+ \\ |1_k\rangle_{\mathcal{M}}^+ &= R(\cos r |1_k\rangle_I^+ |0_{-k}\rangle_{II}^- |0_{-k}\rangle_{II}^- |0_k\rangle_{II}^+ - \sin r |1_k\rangle_I^+ |0_{-k}\rangle_{II}^- |1_{-k}\rangle_{II}^- |1_k\rangle_{II}^+) \\ &\quad + L(\cos r |0_k\rangle_I^+ |0_{-k}\rangle_{II}^- |1_{-k}\rangle_{II}^- |0_k\rangle_{II}^+ + \sin r |1_k\rangle_I^+ |1_{-k}\rangle_{II}^- |0_{-k}\rangle_{II}^- |1_k\rangle_{II}^+) \end{aligned} \tag{11}$$

It has been observed that Minkowski states can be represented using two separate Hilbert spaces for two causally disconnected regions, namely I and II , with positive and negative wave modes. The region that is inaccessible to the observer must be traced over. In our analysis, we consider the scenario where either one (Bob’s qubit) or both observers are simultaneously undergoing acceleration. The restriction of the state to the region I of Rindler coordinates results in the loss of prepared coherence, leading to a mixed state.

When only Bob accelerates, the density matrix (6) of bipartite system in the computational basis is expressed as:

$$\rho_{A\bar{B}} = \rho_{11}^\circ |00\rangle\langle 00| + \rho_{22}^\circ |01\rangle\langle 01| + \rho_{33}^\circ |10\rangle\langle 10| + \rho_{44}^\circ |11\rangle\langle 11| + (\rho_{14}^\circ |00\rangle\langle 11| + H.C.), \tag{12}$$

where ρ_{ij}° are calculated as:

$$\begin{aligned} \rho_{11}^\circ &= \frac{1}{4} \cos(r_b)^2 ((x - 1)|R|^2 + 2), & \rho_{22}^\circ &= \frac{1}{4} (2 \sin(r_b)^2 - \cos(r_b)^2 (x - 1)|R|^2), \\ \rho_{33}^\circ &= -\frac{1}{4} \cos(r_b)^2 ((x + 1)|R|^2 - 2), & \rho_{44}^\circ &= \frac{1}{4} (\cos(r_b)^2 (x + 1)|R|^2 + 2 \sin(r_b)^2) \\ \rho_{14}^\circ &= \frac{1}{2} x R^* \cos(r_b). \end{aligned} \tag{13}$$

Here, r_b denotes the acceleration parameter of Bob, and an asterisk over any parameters denotes the complex conjugation. A bar over each observer slot in this and subsequent subsections, implies that this partner accelerates.

If we assume that Alice’s and Bob’s qubits are accelerated collectively by the parameters of r_a and r_b , respectively. The resulting density matrix of the bipartite system for the accessible region of each observer in Rindler coordinates can be expressed as follows:

$$\rho_{A\bar{B}} = \rho_{11}^* |00\rangle\langle 00| + \rho_{22}^* |01\rangle\langle 01| + \rho_{33}^* |10\rangle\langle 10| + \rho_{44}^* |11\rangle\langle 11| + (\rho_{14}^* |00\rangle\langle 11| + H.C.), \tag{14}$$

where ρ_{ij}^* are calculated as:

$$\begin{aligned}
 \rho_{11}^\bullet &= \frac{1}{4} \cos^2(r_a) \cos^2(r_b) ((x+1)|R|^4 - 4|R|^2 + 4), \\
 \rho_{22}^\bullet &= -\frac{1}{4} \cos^2(r_b) ((x+1)|R|^4 \cos^2(r_a) - 2|R|^2 \cos(2r_a) - 4 \sin^2(r_a)), \\
 \rho_{33}^\bullet &= -\frac{1}{4} \cos^2(r_a) ((x+1)|R|^4 \cos^2(r_b) - 2|R|^2 \cos(2r_b) - 4 \sin^2(r_b)), \\
 \rho_{44}^\bullet &= \frac{1}{8} (2(x+1)|R|^4 \cos^2(r_a) \cos^2(r_b) + 2|R|^2 (\cos(2r_a) \cos(2r_b) + 1) \\
 &\quad + 8 \sin^2(r_a) \sin^2(r_b)), \\
 \rho_{14}^\bullet &= \frac{1}{2} x R^{*2} \cos(r_a) \cos(r_b).
 \end{aligned}
 \tag{15}$$

4 Effect of a classical stochastic noise

Now, we assume that both qubits (specifically, the accessible sector of them) are subjected to interaction with their respective environments. As previously mentioned, we define the environment as a classical stochastic field that manifests as random telegraph noise. The Hamiltonian $\mathcal{H}(t)$ that characterizes the evolution of a bipartite system interacting with a classical environment over a duration of time t can generally be expressed as,

$$\mathcal{H}(t) = \mathcal{H}_A \otimes \mathbb{1} + \mathbb{1} \otimes \mathcal{H}_B,
 \tag{16}$$

where $\mathbb{1}$ represents the identity matrix on a two dimensional Hilbert space and $\mathcal{H}_{A(B)}$ is a single-qubit Hamiltonian describing its dynamics in the presence of noise which can be explicitly written as,

$$\mathcal{H}_{A(B)} = \epsilon \mathbb{1}_{A(B)} + g_{A(B)} \chi_{A(B)}(t) \sigma_{x_{A(B)}}.
 \tag{17}$$

Here, ϵ represents the energy of a qubit in the absence of noise. The qubit-environment coupling strength is denoted by g_i ($i = A, B$) and is measured in units of inverse time. Additionally, $\chi_{A(B)}$ is a characteristic parameter of classical noise that varies randomly. The Pauli spin flip matrix, represented by σ_x , reflects the impact of classical noise on the qubit. As such, this Hamiltonian can effectively describe the stochastic time evolution of a quantum system, as a result the qubit's evolved state to acquire a random phase represented by $\Phi_i(t) = -\gamma \int_0^t \chi_i(t') dt'$. In this paper, the parameter $\chi_i(t)$ represents random telegraph noise (RTN), which randomly fluctuates between ± 1 at a rate of γ . The second-order statistic of RTN is determined by its auto-correlation function $K(t, t')$, which is given by,

$$K(t, t') = \langle \chi(t) \cdot \chi(t') \rangle = e^{-2\gamma t},
 \tag{18}$$

where $\langle \dots \rangle$ denotes the average over all possible realizations of the process $\chi(t)$. The collective impact of the noise on the evolved state can be determined by averaging the resulting density matrix over $\Phi_i(t)$ using,

$$\rho_{AB}^{channel}(t) = \langle U(\chi_A, \chi_B, t) \rho_{AB} U^\dagger(\chi_A, \chi_B, t) \rangle,
 \tag{19}$$

here, $U(\chi_A, \chi_B, t)$ is the unitary operator for time evolution of the Hamiltonian (16) can be expressed as $U(\chi_A, \chi_B, t) = \exp[-i \int \mathcal{H}(t) dt]$, where $\hbar = 1$. Depending on the switching rate and coupling strength with the environment, the noise behavior can exhibit either

Markovian or non-Markovian characteristics. For $\Gamma \equiv \gamma/g \gg 1$, which is referred to as the weak coupling regime, a Markovian regime is observed. Conversely, for $\Gamma \equiv \gamma/g \ll 1$, known as the strong coupling regime, non-Markovian behavior is observed (Bordone et al. 2013). In this study, we consider two cases: (i) both qubits interact with a common environment, where $\chi_A = \chi_B = \chi$ and $g_A = g_B = g$; and (ii) each observer interacts independently with their own environment. In the subsequent sections, we present the density matrix of systems that correspond to different scenarios of accelerated states in the presence of classical stochastic noise.

4.1 The accelerated systems are interacted with a stochastic common environment

By utilizing the computational outlined of accelerated systems in Sect. 3, we can derive the density matrix of a system subject to varying acceleration within a shared environment. Furthermore, we will investigate the impact of this noise channel on both entanglement and the negative values of atomic Wigner function.

4.1.1 If Bob’s qubit is only accelerated

Firstly, it is assumed that Bob’s qubit is subjected to acceleration and the system as a whole is compelled to interact with a stochastic common environment. The resulting density matrix of the system at any given time t can be obtained as follows,

$$\begin{aligned} \rho_{AB}^{com}(t) = & \rho_{11}^{c1} |00\rangle\langle 00| + \rho_{22}^{c1} |01\rangle\langle 01| + \rho_{33}^{c1} |10\rangle\langle 10| + \rho_{44}^{c1} |11\rangle\langle 11| \\ & + (\rho_{23}^{c1} |01\rangle\langle 10| + \rho_{14}^{c1} |00\rangle\langle 11| + H.C.), \end{aligned} \tag{20}$$

with array components as:

$$\begin{aligned} \rho_{11}^{c1} = & A_1 + A_2 \mathcal{D}_2(\tau, \gamma) + A_3 \mathcal{D}_4(\tau, \gamma), & \rho_{22}^{c1} = & A_4 - A_2 \mathcal{D}_2(\tau, \gamma) - A_3 \mathcal{D}_4(\tau, \gamma), \\ \rho_{33}^{c1} = & A_4 + A_2 \mathcal{D}_2(\tau, \gamma) - A_3 \mathcal{D}_4(\tau, \gamma), & \rho_{44}^{c1} = & A_1 - A_2 \mathcal{D}_2(\tau, \gamma) + A_3 \mathcal{D}_4(\tau, \gamma), \\ \rho_{14}^{c1} = & A_5 + A_6 \mathcal{D}_2(\tau, \gamma) + A_3 \mathcal{D}_4(\tau, \gamma), & \rho_{23}^{c1} = & A_3 (1 - \mathcal{D}_4(\tau, \gamma)), \end{aligned}$$

where A_i are given by:

$$\begin{aligned} A_1 = & \frac{1}{8} (x|R|^2 \cos^2(r_b) - x \operatorname{Re}[R] \cos(r_b) + 2), & A_2 = & \frac{1}{4} (\cos(2r_b) - \cos^2(r_b)|R|^2) \\ A_3 = & \frac{1}{8} (x|R|^2 \cos^2(r_b) + x \operatorname{Re}[R] \cos(r_b), & A_4 = & \frac{1}{8} (-x|R|^2 \cos^2(r_b) + x \operatorname{Re}[R] \cos(r_b) + 2) \\ A_5 = & \frac{1}{8} x \cos(r_b) (3\operatorname{Re}[R] - \cos(r_b)|R|^2), & A_6 = & \frac{1}{2} - ix \operatorname{Im}[R] \cos(r_b) \end{aligned}$$

$\mathcal{D}_n(t, \gamma)$ corresponds to the average phase factor $e^{in\phi}$, which appears through time evolution and it is calculated as (Abel and Marquardt 2008):

$$\mathcal{D}_n(t, \gamma) = \begin{cases} e^{-\gamma t} \left(\cosh \delta_{ng} t + \frac{\gamma}{\delta_{ng}} \sinh \delta_{ng} t \right) & \gamma > ng \\ e^{-\gamma t} \left(\cos \delta_{ng} t + \frac{\gamma}{\delta_{ng}} \sin \delta_{ng} t \right) & \gamma < ng \end{cases} \tag{21}$$

where $\delta_{ng} = \sqrt{|\gamma^2 - (ng)^2|}$. The Wigner function Eq. (5) in this case is given by,

$$\begin{aligned}
 \mathcal{W}_{\rho_{AB}^{com}(t)} = \min \left\{ 0, \frac{1}{16} |\mathbf{R}|^2 \cos^2(r_b) \left(4\sqrt{3} \cos(\theta) \mathcal{D}_2(\tau, \gamma) - 3x \cos^2(\theta) (\cos(2\phi) (\mathcal{D}_4(\tau, \gamma) - 1) \right. \right. \\
 - 3\mathcal{D}_4(\tau, \gamma) - 1) - 6x \sin^2(\phi) (\mathcal{D}_4(\tau, \gamma) - 1) \Big) \\
 - \frac{3}{4} x \sin^2(\theta) \text{Im}[\mathbf{R}] \cos(r_b) \sin(2\phi) \mathcal{D}_2(\tau, \gamma) \\
 + \frac{1}{16} \left(4 - 4\sqrt{3} \cos(\theta) \cos(2r_b) \mathcal{D}_2(\tau, \gamma) \right) \\
 - \frac{3}{16} x \cos(r_b) \text{Re}[\mathbf{R}] \left(-(1 - \cos^2(\theta)) \cos(2\phi) (\mathcal{D}_4(\tau, \gamma) + 3) \right. \\
 \left. \left. + \cos^2(\theta) (3 - 3\mathcal{D}_4(\tau, \gamma)) + \mathcal{D}_4(\tau, \gamma) - 1 \right) \right\} \tag{22}
 \end{aligned}$$

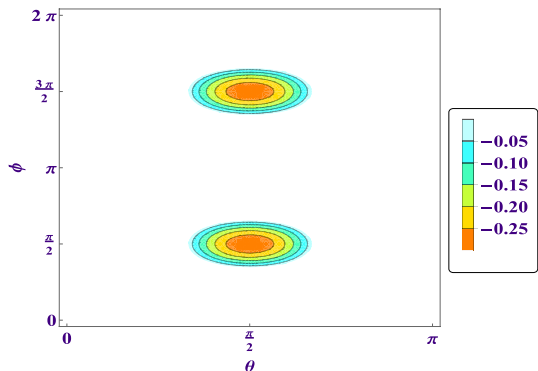
In Fig. 1, we present the contour plot of the negative values of Wigner function of the output state (20) on the (θ, ϕ) plane. It is assumed that the initial state (6) is maximally entangled state with $x = 1$, the acceleration parameter $r_b = 0.1$, the scaled time $\tau = \pi$, $\Gamma = 0.1$, and $|\mathbf{R}| = 1$. The negative values of the Wigner function are observed to form circular patterns around $(\phi, \theta) = (\pi/2, \pi/2)$ and $(\pi/2, 3\pi/2)$, indicating that quantum correlation can be captured in these regions. Hence, we can choose suitable values of θ and ϕ at these points in the presence of the stochastic common environment to explore quantum correlation. Computational analysis reveals that the acceleration of the qubit results in a decrease in the lower limits of the Wigner function (Abd-Rabbou et al. 2019). We will provide a comprehensive explanation of this phenomenon in the following section.

4.1.2 If two qubits are accelerated simultaneously

Let us consider the accelerated two-qubit system with density matrix given by Eq. (14) is forced to interact with a classical stochastic common environment. The evolved density operator $\rho_{AB}^{com}(t)$ at any time t can be calculated using Eq. (19) as follows,

$$\begin{aligned}
 \rho_{AB}^{com}(t) = \rho_{11}^{c2} |00\rangle\langle 00| + \rho_{22}^{c2} |01\rangle\langle 01| + \rho_{33}^{c2} |10\rangle\langle 10| + \rho_{44}^{c2} |11\rangle\langle 11| \\
 \rho_{23}^{c2} + |01\rangle\langle 10| (\rho_{14}^{c2} |00\rangle\langle 11| + H.C.), \tag{23}
 \end{aligned}$$

Fig. 1 The contour plot of the Wigner function in (θ, ϕ) surface for the output state (20) with $x = 1, \tau = \pi, \Gamma = 0.1, r_b = 0.1,$ and $\mathbf{R} = 1$



where the elements are calculated as:

$$\begin{aligned} \rho_{11}^{c2} &= B_1 + B_2 \mathcal{D}_2(\tau, \gamma) + B_3 \mathcal{D}_4(\tau, \gamma), & \rho_{22}^{c2} &= B_4 + B_5 \mathcal{D}_2(\tau, \gamma) + B_6 \mathcal{D}_4(\tau, \gamma), \\ \rho_{33}^{c2} &= B_4 - B_5 \mathcal{D}_2(\tau, \gamma) + B_6 \mathcal{D}_4(\tau, \gamma), & \rho_{44}^{c2} &= B_1 - B_2 \mathcal{D}_2(\tau, \gamma) + B_3 \mathcal{D}_4(\tau, \gamma), \\ \rho_{14}^{c2} &= B_7 + B_8 \mathcal{D}_2(\tau, \gamma) + B_3 \mathcal{D}_4(\tau, \gamma), & \rho_{23}^{c2} &= B_3 - B_3 \mathcal{D}_4(\tau, \gamma), \end{aligned}$$

with

$$\begin{aligned} B_1 &= b_1 - b_3 - b_2 + b_4, & B_2 &= \frac{-1}{8} |R|^2 (\cos(2r_a) + \cos(2r_b) + 2) + \frac{1}{4} (\cos(2r_a) + \cos(2r_b)) \\ B_3 &= b_1 - b_3 + b_2 + b_5, & B_4 &= -B_1, & B_5 &= \frac{1}{8} (|R|^2 - 2) (\cos(2r_a) - \cos(2r_b)) \\ B_6 &= -B_3, & B_7 &= -b_1 + b_3 + 3b_2 - b_5, & B_8 &= \frac{1}{4} x \left((R^*)^2 - R^2 \right) \cos(r_a) \cos(r_b) \end{aligned}$$

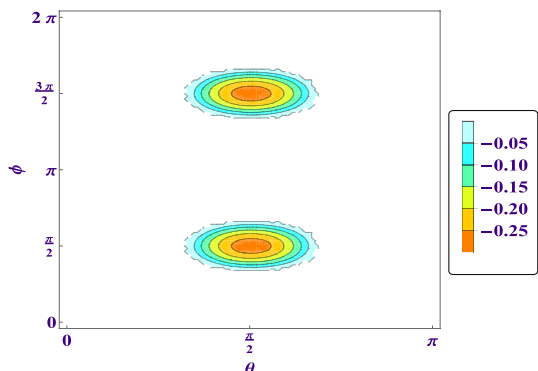
and

$$\begin{aligned} b_1 &= \frac{1}{8} (x + 1) |R|^4 \cos(r_a)^2 \cos(r_b)^2, & b_2 &= \frac{1}{16} x \left((R^*)^2 + R^2 \right) \cos(r_a) \cos(r_b), \\ b_3 &= \frac{1}{16} |R|^2 (\cos(2r_a) (2 \cos(2r_b) + 1) + \cos(2r_b)), \\ b_4 &= \frac{1}{16} (\cos(2r_a - 2r_b) + \cos(2(r_a + r_b)) + 4) \\ b_5 &= \frac{1}{8} \cos(2r_a) \cos(2r_b), \end{aligned}$$

The negative Wigner function behaviour of the output density state (23) is illustrated in Fig. 2. A comparison between Figs. 1 and 2 highlight the impact of the Unruh effect on quantum correlations among observers. Specifically, the region with negative Wigner function values is more confined in Fig. 2 than in Fig. 1. Since the general form of Wigner function in this cases is complicated, so, we present Wigner function with substitution the values $\theta = \phi = \pi/2$. This choice for θ, ϕ can be justified numerically as depicted in Fig. 2.

For these values of θ and ϕ , the Wigner functions can gain the minimum values over the whole allowed range. With this remark, we can write,

Fig. 2 The contour plot of the Wigner function in (θ, ϕ) surface for the output state (23) with $x = 1, \tau = \pi, \Gamma = 0.1,$ $r_a = r_b = 0.1,$ and $R = 1$



$$\begin{aligned}
 \mathcal{W}_{\rho_{AB}^{com}(t)} = \min & \left\{ 0, \frac{3}{16} |\mathbf{R}|^2 (\cos(2r_a)(2 \cos(2r_b) + 1) + \cos(2r_b)) (\mathcal{D}_4(\tau, \gamma) - 1) \right. \\
 & + \frac{3}{8} (x + 1) |\mathbf{R}|^4 \cos(r_a)^2 \cos(r_b)^2 (1 - \mathcal{D}_4(\tau, \gamma)) \\
 & + \frac{3}{8} x \cos(r_a) \cos(r_b) (\text{Im}[\mathbf{R}]^2 - \text{Re}[\mathbf{R}]^2) (\mathcal{D}_4(\tau, \gamma) + 1) \\
 & \left. - \frac{3}{4} (\cos(r_a) - \cos(r_b))^2 (\mathcal{D}_4(\tau, \gamma) + 1) + \frac{5}{8} - \frac{3}{8} \mathcal{D}_4(\tau, \gamma) \right\}
 \end{aligned} \tag{24}$$

4.2 The accelerated systems are interacted independently with their own stochastic environment

In this subsection, we assume that the subsystems are interacted independently with their own stochastic environments. In addition, either Bob’s qubit is individually accelerated or two qubits are accelerated simultaneously. So, we will treat these two cases in the following, separately.

4.2.1 If Bob’s qubit is only accelerated

When subsystems are brought to interact independently with their own stochastic environments, the initial density matrix (12) will evolve to:

$$\begin{aligned}
 \rho_{AB}^{in}(t) = & \rho_{11}^{d1} |00\rangle\langle 00| + \rho_{22}^{d1} |01\rangle\langle 01| + \rho_{33}^{d1} |10\rangle\langle 10| \\
 & + \rho_{44}^{d1} |11\rangle\langle 11| + (\rho_{23}^{d1} |01\rangle\langle 10| \rho_{14}^{d1} |00\rangle\langle 11| + H.C.),
 \end{aligned}$$

with array components as:

$$\begin{aligned}
 \rho_{11}^{d1} &= \frac{1}{4} (1 + C_1 \mathcal{D}_2(\tau, \gamma_2) + C_2 \mathcal{D}_2(\tau, \gamma_1) \mathcal{D}_2(\tau, \gamma_2)), \\
 \rho_{22}^{d1} &= \frac{1}{4} (1 - C_1 \mathcal{D}_2(\tau, \gamma_2) - C_2 \mathcal{D}_2(\tau, \gamma_1) \mathcal{D}_2(\tau, \gamma_2)) \\
 \rho_{33}^{d1} &= \frac{1}{4} (1 + C_1 \mathcal{D}_2(\tau, \gamma_2) - C_2 \mathcal{D}_2(\tau, \gamma_1) \mathcal{D}_2(\tau, \gamma_2)) \\
 \rho_{44}^{d1} &= \frac{1}{4} (1 - C_1 \mathcal{D}_2(\tau, \gamma_2) + C_2 \mathcal{D}_2(\tau, \gamma_1) \mathcal{D}_2(\tau, \gamma_2)) \\
 \rho_{14}^{d1} &= C_3 (1 + \mathcal{D}_2(\tau, \gamma_1) \mathcal{D}_2(\tau, \gamma_2)) + C_4 (\mathcal{D}_2(\tau, \gamma_1) + \mathcal{D}_2(\tau, \gamma_2)) \\
 \rho_{23}^{d1} &= C_3 (1 - \mathcal{D}_2(\tau, \gamma_1) \mathcal{D}_2(\tau, \gamma_2)) + C_4 (\mathcal{D}_2(\tau, \gamma_1) - \mathcal{D}_2(\tau, \gamma_2))
 \end{aligned}$$

where C_i are:

$$\begin{aligned}
 C_1 &= \cos(2r_b) - |\mathbf{R}|^2 \cos(r_b)^2, \quad C_2 = \frac{1}{4} x |\mathbf{R}|^2 \cos(r_b)^2, \\
 C_3 &= \frac{1}{4} x \text{Re}[\mathbf{R}] \cos(r_b), \quad C_4 = -\frac{i}{4} x \text{Im}[\mathbf{R}] \cos(r_b)
 \end{aligned} \tag{25}$$

where $\mathcal{D}_2(t, \gamma_i)$ is obtained from Eq. (21), and $\gamma_{1(2)}$ refers to Alice (Bob)’s environment noise rate. The Wigner function in this case take the following form:

$$\begin{aligned}
 \mathcal{W}_{\rho_{AB}^{in}(t)} = \min \left\{ 0, \frac{1}{4} |R|^2 \cos(\theta) \cos(r_b)^2 \mathcal{D}_2(\tau, \gamma_2) \left(3x \cos(\theta) \mathcal{D}_2(\tau, \gamma_1) + \sqrt{3} \right) \right. \\
 - \frac{3}{8} x \sin^2(\theta) \operatorname{Im}[R] \cos(r_b) \sin(2\phi) (\mathcal{D}_2(\tau, \gamma_1) + \mathcal{D}_2(\tau, \gamma_2)) \\
 + \frac{1}{8} \left(2 - 2\sqrt{3} \cos(\theta) \cos(2r_b) \mathcal{D}_2(\tau, \gamma_2) \right) \\
 + \frac{3}{8} x \sin^2(\theta) \cos(r_b) \operatorname{Re}[R] (\cos(2\phi) (\mathcal{D}_2(\tau, \gamma_1) \mathcal{D}_2(\tau, \gamma_2) + 1) \\
 \left. - \mathcal{D}_2(\tau, \gamma_1) \mathcal{D}_2(\tau, \gamma_2) + 1) \right\} \tag{26}
 \end{aligned}$$

Similarly to Fig. 1, the contour plot of the Wigner function for the accelerated state (Eq. 25) is presented in Fig. 3. In this case, Bob’s qubit is only accelerated with $r_b = 0.1$, and the decoherence parameters of both baths are equal, with $\Gamma_a = \Gamma_b = 0.1$. The minimum bounds of the Wigner function are lower than those displayed in Fig. 1, indicating that the independent stochastic environment dissipates quantum correlation faster than the common environment. Furthermore, maximum bounds of quantum correlation accumulate at $(\phi, \theta) = (\pi/2, \pi/2)$ and $(\pi/2, 3\pi/2)$, making these points suitable for capturing the quantum correlation of the state in the Wigner function.

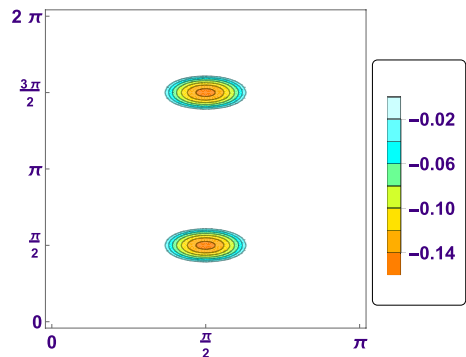
4.2.2 If two qubits are accelerated simultaneously

Beginning from the initial density matrix Eq. (14), the evolved density matrix is calculated as:

$$\begin{aligned}
 \rho_{AB}^{in}(t) = \rho_{11}^{d2} |00\rangle\langle 00| + \rho_{22}^{d2} |01\rangle\langle 01| + \rho_{33}^{d2} |10\rangle\langle 10| + \rho_{44}^{d2} |11\rangle\langle 11| \\
 + (\rho_{23}^{d2} |01\rangle\langle 10| + H.C.) + (\rho_{14}^{d2} |00\rangle\langle 11| + H.C.), \tag{27}
 \end{aligned}$$

with

Fig. 3 The contour plot of the Wigner function in (θ, ϕ) surface for the output state (25) with the same parameters as displayed in Fig. 1



$$\begin{aligned} \rho_{11}^{d2} &= \frac{1}{4}(1 + \mathcal{G}_1 \mathcal{D}_2(\tau, \gamma_1) + \mathcal{G}_2 \mathcal{D}_2(\tau, \gamma_2) + \mathcal{G}_3 \mathcal{D}_2(\tau, \gamma_1) \mathcal{D}_2(\tau, \gamma_2)) \\ \rho_{22}^{d2} &= \frac{1}{4}(1 + \mathcal{G}_1 \mathcal{D}_2(\tau, \gamma_1) - \mathcal{G}_2 \mathcal{D}_2(\tau, \gamma_2) - \mathcal{G}_3 \mathcal{D}_2(\tau, \gamma_1) \mathcal{D}_2(\tau, \gamma_2)) \\ \rho_{33}^{d2} &= \frac{1}{4}(1 - \mathcal{G}_1 \mathcal{D}_2(\tau, \gamma_1) + \mathcal{G}_2 \mathcal{D}_2(\tau, \gamma_2) - \mathcal{G}_3 \mathcal{D}_2(\tau, \gamma_1) \mathcal{D}_2(\tau, \gamma_2)) \\ \rho_{44}^{d2} &= \frac{1}{4}(1 - \mathcal{G}_1 \mathcal{D}_2(\tau, \gamma_1) - \mathcal{G}_2 \mathcal{D}_2(\tau, \gamma_2) + \mathcal{G}_3 \mathcal{D}_2(\tau, \gamma_1) \mathcal{D}_2(\tau, \gamma_2)) \\ \rho_{14}^{d2} &= (\mathcal{G}_4 + \mathcal{G}_5 \mathcal{D}_2(\tau, \gamma_1) + \mathcal{G}_5 \mathcal{D}_2(\tau, \gamma_2) + \mathcal{G}_4 \mathcal{D}_2(\tau, \gamma_1) \mathcal{D}_2(\tau, \gamma_2)) \\ \rho_{23}^{d2} &= (\mathcal{G}_4 + \mathcal{G}_5 \mathcal{D}_2(\tau, \gamma_1) - \mathcal{G}_5 \mathcal{D}_2(\tau, \gamma_2) - \mathcal{G}_4 \mathcal{D}_2(\tau, \gamma_1) \mathcal{D}_2(\tau, \gamma_2)) \end{aligned}$$

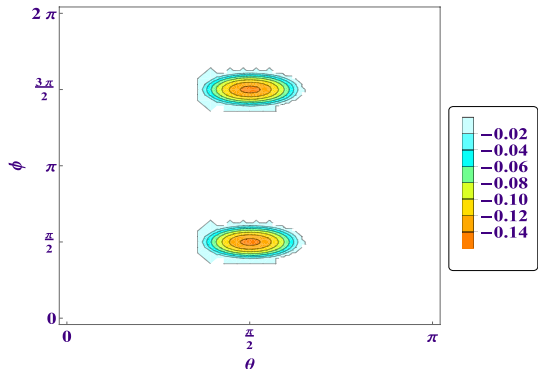
where \mathcal{G}_i are:

$$\begin{aligned} \mathcal{G}_1 &= \frac{1}{4} \cos(2r_b) - \frac{1}{4} |\mathbf{R}|^2 \cos(r_b)^2, & \mathcal{G}_2 &= \frac{1}{4} \cos(2r_a) - \frac{1}{4} |\mathbf{R}|^2 \cos(r_a)^2 \\ \mathcal{G}_3 &= \frac{1}{4} (x + 1) |\mathbf{R}|^4 \cos(r_a)^2 \cos(r_b)^2 - \frac{1}{8} |\mathbf{R}|^2 (\cos(2r_a)(2 \cos(2r_b) + 1) + \cos(2r_b)) \\ &\quad + \frac{1}{4} \cos(2r_a) \cos(2r_b) \\ \mathcal{G}_4 &= \frac{1}{8} x \left((\mathbf{R}^*)^2 + \mathbf{R}^2 \right) \cos(r_a) \cos(r_b), & \mathcal{G}_5 &= \frac{1}{8} x \left((\mathbf{R}^*)^2 - \mathbf{R}^2 \right) \cos(r_a) \cos(r_b) \end{aligned} \tag{28}$$

Likewise, Fig. 4 illustrates that the Wigner function is centered at identical points for the preceding three scenarios. Here, we accelerated the initial two-qubit system and allowed them to interact independently with their respective stochastic noise. The center orange region is smaller than in the previous three cases, indicating independent environment decoherence of non-classical correlation. Furthermore, acceleration parameters exacerbate this decoherence.

For the output state (27), we obtained the Wigner function by substituting $\theta = \phi = \pi/2$. This parameter selection is justified by Fig. 4, which indicates that these specific values of θ and ϕ correspond to the minimum values of the Wigner function. Consequently, the Wigner function reads,

Fig. 4 The contour plot of the Wigner function in (θ, ϕ) surface for the output state (27) with the same parameters as displayed in Fig. 2



$$\mathcal{W}_{\rho_{AB}^{in}(t)} = \min \left\{ 0, \frac{1}{4} (3x \cos(r_a) \cos(r_b) (\text{Im}[\mathbf{R}]^2 - \text{Re}[\mathbf{R}]^2) \mathcal{D}_2(\tau, \gamma_1) \mathcal{D}_2(\tau, \gamma_2) + 1) \right\} \tag{29}$$

5 The quantum correlations and the entanglements: the results

Since the existence of quantum correlation in a system can be designated by the negative corresponding Wigner function, it is helpful to determine the sign of these functions. By solving the Eqs. (22, 24, 26, 29) in term of x , we get the following roots for the Wigner functions:

$$\begin{aligned} x_0^{\mathcal{W}_1} &= \frac{4}{3(2|\mathbf{R}|^2 \cos^2(r_b) (\mathcal{D}_4(\tau, \gamma) - 1) + 2 \cos(r_b) \text{Re}[\mathbf{R}] (\mathcal{D}_4(\tau, \gamma) + 1))}, \\ x_0^{\mathcal{W}_2} &= \left(\sec(r_a) \sec(r_b) \left(6(1 - \mathcal{D}_4(\tau, \gamma)) (|\mathbf{R}|^2 \cos^2(r_b) (|\mathbf{R}|^2 \cos^2(r_a) - \cos(2r_a)) \right. \right. \\ &\quad \left. \left. + \cos(2r_b) (\cos(2r_a) - |\mathbf{R}|^2 \cos^2(r_a)) \right) + 4 \right) / \\ &\quad \left(6|\mathbf{R}|^4 \cos(r_a) \cos(r_b) (\mathcal{D}_4(\tau, \gamma) - 1) + 3(\text{Im}[\mathbf{R}]^2 + \text{Re}[\mathbf{R}]^2) (\mathcal{D}_4(\tau, \gamma) + 1) \right), \\ x_0^{\mathcal{W}_3} &= \frac{\sec(r_b)}{3\text{Re}[\mathbf{R}] \mathcal{D}_2(\tau, \gamma_1) \mathcal{D}_2(\tau, \gamma_2)} \\ x_0^{\mathcal{W}_4} &= \frac{\sec(r_a) \sec(r_b)}{3(\text{Re}[\mathbf{R}]^2 - \text{Im}[\mathbf{R}]^2) \mathcal{D}_2(\tau, \gamma_1) \mathcal{D}_2(\tau, \gamma_2)}, \end{aligned} \tag{30}$$

where we have abbreviated $\mathcal{W}_{\rho_{AB}^{com}(t)}$, $\mathcal{W}_{\rho_{AB}^{com}(t)}$, $\mathcal{W}_{\rho_{AB}^{in}(t)}$ and $\mathcal{W}_{\rho_{AB}^{in}(t)}$, by \mathcal{W}_1 , \mathcal{W}_2 , \mathcal{W}_3 and \mathcal{W}_4 , respectively. We will also use this for easiness hereafter. For the later convenient, we will denote \mathcal{C}_1 , \mathcal{C}_2 , \mathcal{C}_3 , \mathcal{C}_4 , as the corresponding concurrences for four cases in Sec. (4).

In order to demonstrate the efficacy of the Wigner function in elucidating quantitative correlations, appropriate figures will be presented for comparison with concurrence. Figure 5a exhibits the Wigner function (\mathcal{W}) and concurrence (\mathcal{C}) as a function of the initial state’s purity parameter x , for specific values of τ , Γ , and r as indicated in the caption.

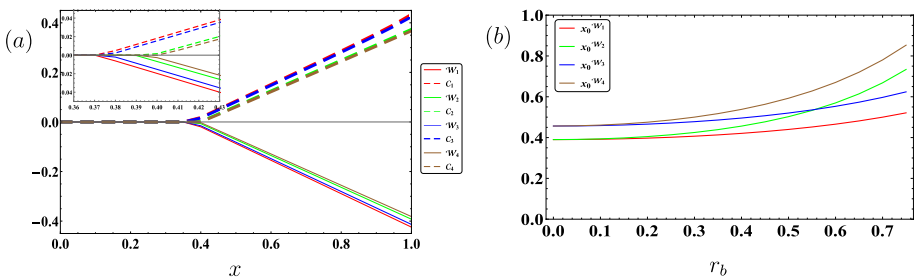


Fig. 5 **a** Comparison of four situations of the Wigner functions and concurrences against x with the specified parameters $\tau = \pi/2$, $\Gamma = \Gamma_1 = \Gamma_2 = 0.05$, and $r_b = 0.3$, $r_a = 0.4$ and $\mathbf{R} = 1$. The inset attached shows the detail of the plots around $x \approx 0.4$, **b** the roots of the Wigner functions for four cases with $\Gamma = \Gamma_1 = \Gamma_2 = 0.01$, $r_a = r_b$, $x = 0.95$, $\tau = \pi/2$, $\mathbf{R} = 1$

Throughout our discussion, we presume that the distribution angles are fixed at $\theta = \phi = \frac{\pi}{2}$, where this point is related to the minimum value of the Wigner function in phase space. We consider the single mode approximation, $R = 1$ for now. Later we will discard this approximation, and discuss on its effect on the correlations between observers.

It is inferred that to maintain the initial quantum correlation among observers, the value of x must exceed a certain threshold. Figure 5a illustrates that the system’s interaction with the environment is crucial in characterizing the correlation for specific parameters. Although for small values of accelerations the common environment condition provides a greater amount of correlations between observers, but by increasing the acceleration, the Unruh effect plays a prominent role to suppress quantum correlations. Indeed, for arbitrary values of acceleration, the status of observers concerning the inertial reference frame is determinative. For systems with equal initial conditions and noise strength, those with only accelerating observers exhibit more significant correlations than those with both accelerating and non-accelerating observers, regardless of any imposed noise configuration. Under this conditions, the lower bounds of the functions \mathcal{W}_1 and \mathcal{W}_3 exceed those of \mathcal{W}_2 and \mathcal{W}_4 , respectively. This trend is also observed in the corresponding concurrences. The impact of acceleration on correlations becomes evident when comparing either \mathcal{W}_1 and \mathcal{W}_3 , or \mathcal{W}_2 and \mathcal{W}_4 . Notably, when two observers accelerate simultaneously, the correlation decreases more significantly than when only one observer accelerates. Therefore, for a non-inertial frame, it is advisable to provide them with a collective environment. Pure states are necessary to achieve high-quality quantum communication between both accelerating observers. To clarify the aforementioned statement, we have plotted the roots of the Wigner function for variable x , as given by Eq. (30), against the parameter r_b in Fig. 5b. It is noteworthy that we have set $r_a = r_b$ for both cases discussed in Sects. 4.2.2 and 4.1.2. Our analysis reveals that as the acceleration increases, a purer state should be shared among the observers to maintain correlation. Furthermore, in cases where there is an independent environment, decoherence effects are more pronounced, necessitating a pure initial density matrix.

A comparative study was conducted between the common and independent stochastic environments of accelerated states with respect to the acceleration parameter r_b , as depicted in Fig. 6. Here, $\tau = \pi$ and $\Gamma = \Gamma_1 = \Gamma_2 = 0.05$. As Bob’s qubit is only accelerated, Fig. 6a illustrates that the functions $\mathcal{W}_1, \mathcal{W}_3, C_1$, and C_3 degrade to a non-zero value at the infinite acceleration limit ($r_b \rightarrow \frac{\pi}{4}$). The common noise configuration is more challenging to overcome than the independent noise configuration, where C_1 is greater than C_3 . Wigner’s

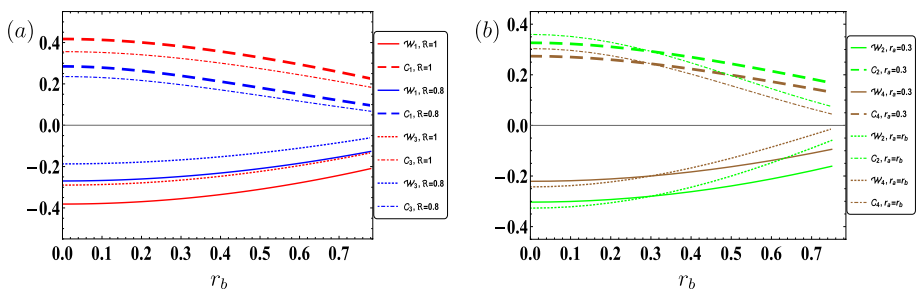


Fig. 6 The effect of common or independent noise configurations on the quantum correlations against the acceleration parameter r_b , with the parameters $\tau = \pi, x = 0.9, \Gamma = \Gamma_1 = \Gamma_2 = 0.05$, **a** only Bob’s qubit is accelerated ($r_a = 0$); the thick line correspond to $R = 1$ and the thin line to $R = 0.85$, **b** two qubits are accelerated with $r_a = 0.3$ or $r_a = r_b$ which have specified in the corresponding legend; $R = 1$ has been considered

function provides an excellent indication of quantum correlation. Furthermore, the impact of disregarding the single mode approximation on the correlations of the states can be inferred from the blue curves in the same sub-figure. These curves correspond to a value of $R = 0.85$. We incorporate the contribution of spacetime modes that are inaccessible to construct the Unruh mode. Consequently, by tracing over these inaccessible region modes, we forfeit this contribution and consequently more prepared correlations are lost due to the Unruh effect. To investigate the Unruh effect on systems with accelerating observers, Fig. 6b has been generated. The relevant quantities in this context are $\mathcal{W}_2, \mathcal{W}_4, \mathcal{C}_2,$ and \mathcal{C}_4 . As depicted in the figure, the quantum correlations and entanglements, namely $\mathcal{W}_2, \mathcal{W}_4, \mathcal{C}_2,$ and \mathcal{C}_4 , exhibit the deepest decay when both qubits are accelerated with identical values ($r_a = r_b$), as compared to when only the Alice qubit is accelerated with a constant value ($r_a = 0.3$). Moreover, it is observed that the decoherence effect of the common noise environment is less pronounced than that of the independent environment.

To demonstrate the impact of different types of noise on the behavior of correlation functions with respect to the decoherence dimensionless rate Γ , we have presented Fig. 7, where we have set $\Gamma_a = \Gamma_b = \Gamma$. For small acceleration parameters (i.e., $r_a = r_b = 0.1$) and $R = 1$, Fig. 7a, b show that the correlation functions, namely $\mathcal{W}_1, \mathcal{W}_2, (\mathcal{C}_1,$ and $\mathcal{C}_2)$, as well as the pair of \mathcal{W}_3 and $\mathcal{W}_4, (\mathcal{C}_3,$ and $\mathcal{C}_4)$, are nearly the same for large values of Γ .

In the Markovian regime, characterized by large values of Γ , the Wigner function and concurrence of a common environment configuration are smaller than those of an independent environment configuration. Specifically, $\mathcal{W}_{1,2} < \mathcal{W}_{3,4}$ and $\mathcal{C}_{1,2} < \mathcal{C}_{3,4}$. Conversely, for small values of Γ , the opposite is true. This observation is supported by the inset of Fig. 7a. In addition, in the non-Markovian regime ($0 < \Gamma < 1$, inset of Fig. 7a), quantum entanglement (\mathcal{C}) extends over a wider range of Γ than quantum correlation as evidenced by the Wigner function (\mathcal{W}). Therefore, we can conclude that the Wigner function is more susceptible to noise than concurrence. Another interesting phenomenon is the occurrence of quiescence in quantum entanglement due to variations in Γ , which can be attributed to a transition from a Markovian to a non-Markovian regime of noise. Figure 7b displays the same quantities as Fig. 7a, except when the single mode approximation ($R = 0.85$) is not applied. The inset of this figure reveals that correlations degrade more rapidly than in the case where the single-mode approximation is used. Under these conditions, the Unruh effect can be amplified by the acceleration of observers. Specifically, Fig. 7b demonstrates that the curves in Fig. 7a, which were nearly identical, deviate significantly from each other.

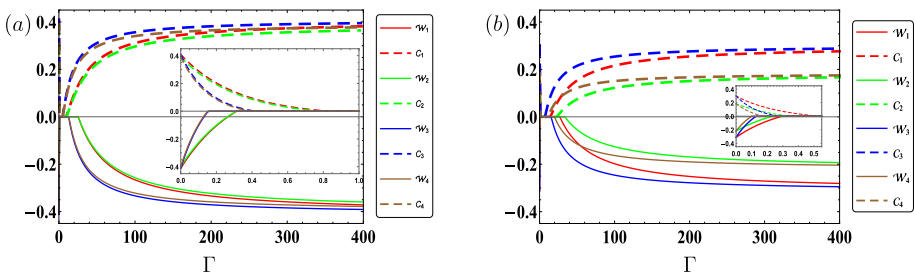


Fig. 7 The behaviour of correlation functions \mathcal{W}_i and \mathcal{C}_i against the rate Γ with the parameters $\tau = \pi, x = 1,$ and $\Gamma = \Gamma_1 = \Gamma_2, r_a = r_b = 0.1, \mathbf{a} R = 1, \mathbf{b} R = 0.85$. The inset in each subfigure display the corresponding plot for $0 < \Gamma < 1$

The behaviour of the correlation function with respect to the dimensionless time $\tau \equiv t g$ is presented in Fig. 8. Figure 8a, b depict the non-Markovian regime ($\Gamma \ll 1$) of noise. In Fig. 8a, the single mode approximation is assumed, while this assumption is discarded in Fig. 8b with $R = 0.85$. A characteristic of the non-Markovian regime is a successive death and rebirth of correlation with damping amplitude. However, Wigner functions undergo deeper degradation in amplitude than entanglement. It is evident from Fig. 8a that correlations contained in systems with common environment configurations are more sensitive to noise than those displayed for the independent environments. Additionally, quantum correlation in the system, as witnessed by the Wigner function, may disappear for a period and reappear after a specific time. This collapse in quantum correlation is not observed for quantum entanglement, where oscillatory behaviour is found. The entanglement for common noise configuration varies more severely than independent noise configuration. The same relation between variation of the Wigner function with common environment against independent environments holds. So, when we imposed the subsystems to interact with an independent environment, a delay in the evolution of correlation is exhibited. When the single mode approximation is discarded, the impact of interaction time and acceleration becomes significant, and the Unruh effect distinguishes between systems with a single accelerating observer and those with both observers accelerating. The specifics of this behaviour are illustrated in the inset of the corresponding figures. Significantly, it has been observed that the application of independent noise channels can effectively reduce the frequency of entanglement death and rebirth, thereby increasing the duration of quantum correlations. This can be demonstrated by comparing $C_{1,2}$ with $C_{3,4}$. Unlike the concurrence, the Wigner function for independent environments experiences more periods of inactivity, while the common environment exhibits more rapid variations. This can be illustrated by comparing $\mathcal{W}_{1,2}$ with $\mathcal{W}_{3,4}$. A note on the difference between the Wigner function and

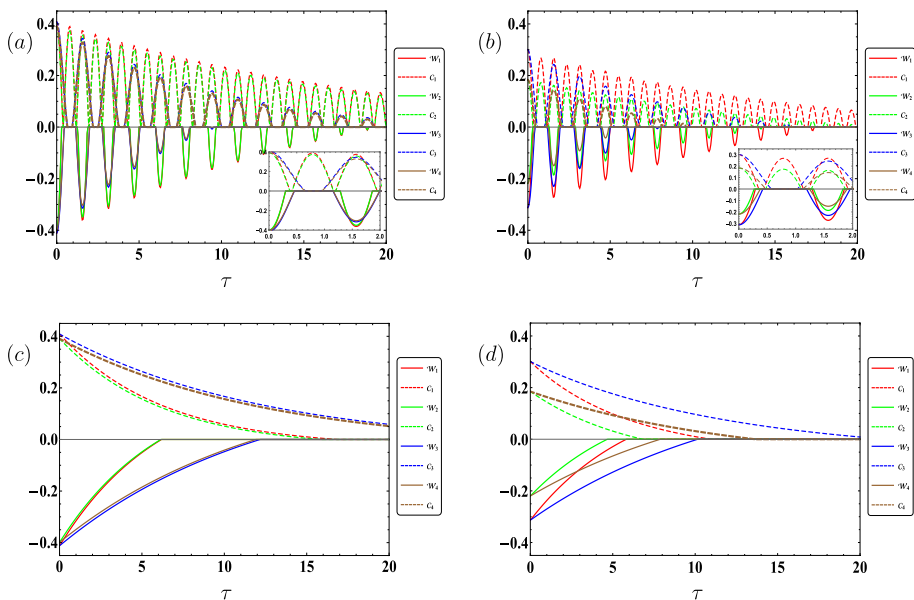


Fig. 8 The behaviour of correlation functions \mathcal{W}_i and C_i against the scaled time τ with the parameters $x = 1$, and $r_a = r_b = 0.1$, **a** $\Gamma = \Gamma_1 = \Gamma_2 = 0.05$, and $R = 1$, **b** the same as **(a)** but $R = 0.85$, **c** $\Gamma = \Gamma_1 = \Gamma_2 = 50$ and $R = 1$, and **d** the same as **(c)** but $R = 0.85$ has been chosen

quantum concurrence would be helpful. Although we have considered the Wigner function as an indicator of non-classical correlations, the quantum concurrence can specifically capture the quantum entanglement of the desired system. Therefore, it is not reasonable to expect that non-classical correlations will accurately reflect quantum entanglement. Interestingly, we have observed instances where the system and environment become separated in time and no correlation exists between them, yet the prepared quantum entanglement remains preserved between them. In Fig. 8c, d, we consider the non-Markovian regime at the other extreme ($\Gamma \gg 1$) for $R = 1$ and $R = 0.85$, respectively. During this time, the correlation decays monotonically with time, but in cases with independent environments, the correlation lasts much longer than in cases with common environment configurations. Figure 8d demonstrates that systems with both accelerating observers have a more fragile correlation than systems with only one accelerating observer.

6 Conclusion

In this study, we have investigated the behaviour of the Wigner function and quantum concurrence in a bipartite mixed entangled state under the influence of RTN and the Unruh effect. Our analysis involved an assessment of the Wigner function and quantum concurrence, and we focused on their behaviour about various parameters such as the purity parameter x , observers' acceleration parameters r_a and r_b , dimensionless evolution time, and dimensionless switching parameter Γ . It is important to note that we did not rely on the single-mode approximation throughout our analysis. Furthermore, we explored how these quantities are affected by different environmental setups, specifically in terms of the independent/ common environment. By comparing our results, we have been able to conclude the behaviour of the Wigner function and quantum concurrence in this context. It has been demonstrated that the concurrence and the negative values of the Wigner function, two non-classical correlation indicators, are compatible with each other. Although the effect of acceleration as a decoherence agent has been established, it has been observed that the configuration of the environment has a more significant and dominant impact on the loss of entanglement and correlations. More intriguingly, it has been noted that quantum correlations and entanglement behave differently for independent and common environments in two regimes of Markovian and non-Markovian noises. Furthermore, by discarding the single-mode approximation, the degradation impact of the Unruh effect on correlations is further strengthened.

Author contributions MYA-R designed the project, developed the theoretical formalism, performed the analytic calculations and the numerical simulations. MS contributed to the design and implementation of the research, to the analysis of the results and to the writing of the manuscript. SK developed the theoretical formalism and contributed to the writing of the manuscript.

Funding Open access funding provided by The Science, Technology & Innovation Funding Authority (STDF) in cooperation with The Egyptian Knowledge Bank (EKB).

Data availability Data availability is not applicable to this article as no new data were created in this study.

Declarations

Conflict of interest The authors declare no competing interests.

Ethical approval The authors declare that there is no conflict with publication ethics.

Open Access This article is licensed under a Creative Commons Attribution 4.0 International License, which permits use, sharing, adaptation, distribution and reproduction in any medium or format, as long as you give appropriate credit to the original author(s) and the source, provide a link to the Creative Commons licence, and indicate if changes were made. The images or other third party material in this article are included in the article's Creative Commons licence, unless indicated otherwise in a credit line to the material. If material is not included in the article's Creative Commons licence and your intended use is not permitted by statutory regulation or exceeds the permitted use, you will need to obtain permission directly from the copyright holder. To view a copy of this licence, visit <http://creativecommons.org/licenses/by/4.0/>.

References

- Abd-Rabbou, M.Y., Metwally, N., Ahmed, M.M.A., Obada, A.-S.F.: Wigner function of noisy accelerated two-qubit system. *Quantum Inf. Process.* **18**(12), 1–19 (2019)
- Abd-Rabbou, M.Y., Metwally, N., Ahmed, M.M.A., Obada, A.S.F.: Wigner distribution of accelerated tripartite W-state. *Optik* **208**, 163921 (2020)
- Abd-Rabbou, M.Y., Khan, S., Shamirzaie, M.: Quantum Fisher information and quantum coherence of an entangled bipartite state interacting with a common classical environment in accelerating frames. *Quantum Inf. Process.* **21**(6), 1–13 (2022)
- Abel, B., Marquardt, F.: Decoherence by quantum telegraph noise: a numerical evaluation. *Phys. Rev. B* **78**, 201302 (2008)
- Abgaryan, V., Khvedelidze, A., Torosyan, A.: Kenfack-życzkowski indicator of nonclassicality for two non-equivalent representations of Wigner function of qutrit. *Phys. Lett. A* **412**, 127591 (2021)
- Agarwal, G.S.: Relation between atomic coherent-state representation, state multipoles, and generalized phase-space distributions. *Phys. Rev. A* **24**, 2889–2896 (1981)
- Agarwal, G.S.: Relation between atomic coherent-state representation, state multipoles, and generalized phase-space distributions. *Phys. Rev. A* **24**, 2889 (1981)
- Arkhipov, I.I., Barasiński, A., Svozilík, J.: Negativity volume of the generalized Wigner function as an entanglement witness for hybrid bipartite states. *Sci. Rep.* **8**(1), 1–11 (2018)
- Bordone, P., Paris, M.G.A., Benedetti, C., Buscemi, F.: Dynamics of quantum correlations in colored environments. *Phys. Rev. A* **87**, 052328 (2013)
- Bruschi, D.E., Louko, J., Martín-Martínez, E., Dragan, A., Fuentes, I.: Unruh effect in quantum information beyond the single-mode approximation. *Phys. Rev. A* **82**, 042332 (2010)
- Chumakov, S.M., Klimov, A.B.: On the SU (2) Wigner function dynamics. *Revista mexicana def sica* **48**, 317–324 (2002)
- Ciampini, M.A., Everitt, M.J., Tilma, T., et al.: Visualizing multiqubit correlations using the Wigner function. *Eur. Phys. J. D* **76**, 90 (2022)
- Dahl, J.P., Mack, H., Wolf, A., Schleich, W.P.: Entanglement versus negative domains of Wigner functions. *Phys. Rev. A* **74**, 042323 (2006)
- Ferrie, C.: Quasi-probability representations of quantum theory with applications to quantum information science. *Rep. Progr. Phys.* **74**(11), 116001 (2011)
- Franco, R., Penna, V.: Discrete Wigner distribution for two qubits: a characterization of entanglement properties. *J. Phys. A Math. Gen.* **39**(20), 5907 (2006)
- Gibbons, K.S., Hoffman, M.J., Wootters, W.K.: Discrete phase space based on finite fields. *Phys. Rev. A* **70**, 062101 (2004)
- Hill, S.A., Wootters, W.K.: Entanglement of a pair of quantum bits. *Phys. Rev. Lett.* **78**, 5022 (1997)
- Husimi, K.: Some formal properties of the density matrix. *Proc. Phys. Math. Soc. Jpn. 3rd Ser.* **22**(4), 264–314 (1940)
- Karlsson, A., Lyyra, H., Laine, E.-M., Mascalco, S., Piilo, J.: Non-Markovian dynamics in two-qubit dephasing channels with an application to superdense coding. *Phys. Rev. A* **93**, 032135 (2016)
- Khan, S., Shamirzaie, M.: The dynamics of quantum correlations and quantum coherence in a classical colored noise. *Phys. Scr.* **95**(10), 105101 (2020)
- Klimov, A.B., Romero, J.L., De Guise, H.: Generalized SU (2) covariant Wigner functions and some of their applications. *J. Phys. A Math. Theor.* **50**(32), 323001 (2017)
- Lo, H.-K., Chau, H.F.: Unconditional security of quantum key distribution over arbitrarily long distances. *Science* **283**(5410), 2050–2056 (1999)

- López, C.C., Paz, J.P.: Phase-space approach to the study of decoherence in quantum walks. *Phys. Rev. A* **68**, 052305 (2003)
- Mavrogordatos, T.K.: Cavity-field distribution in multiphoton Jaynes–Cummings resonances. *Phys. Rev. A* **104**, 063717 (2021)
- McConnell, R., Zhang, H., Jiazhong, H., Čuk, S., Vuletić, V.: Entanglement with negative Wigner function of almost 3,000 atoms heralded by one photon. *Nature* **519**(7544), 439–442 (2015)
- Metwally, N., Abd-Rabbou, M.Y., Obada, A.-S.F., Ahmed, M.M.A.: Wigner function of accelerated and non-accelerated Greenberger–Horne–Zeilinger state. In: 2019 8th International Conference on Modeling Simulation and Applied Optimization (ICMSAO), pp. 1–5 (2019)
- Metwally, N.: Enhancing entanglement, local and non-local information of accelerated two-qubit and two-qutrit systems via weak-reverse measurements. *Europhys. Lett. EPL* **116**(6), 60006 (2017)
- Metwally, N.: Quantum filtering of accelerated qubit-qutrit system. *Optik* **178**, 524–531 (2019)
- Metwally, N., Ebrahim, F.: Fisher information of accelerated two-qubit system in the presence of the color and white noisy channels. *Int. J. Mod. Phys. B* **34**(05), 2050027 (2020)
- Miquel, C., Paz, J.P., Saraceno, M.: Quantum computers in phase space. *Phys. Rev. A* **65**, 062309 (2002)
- Mohamed, A.-B.A., Metwally, N.: Nonclassical features of two SC-qubit system interacting with a coherent SC-cavity. *Phys. E Low-dimens. Syst. Nanostruct.* **102**, 1–7 (2018)
- Moya-Cessa, H., Knight, P.L.: Series representation of quantum-field quasiprobabilities. *Phys. Rev. A* **48**, 2479–2481 (1993)
- Paz, J.P., Roncaglia, A.J., Saraceno, M.: Quantum algorithms for phase-space tomography. *Phys. Rev. A* **69**, 032312 (2004)
- Rahman, A.U., Haddadi, S., Pourkarimi, M.R.: Tripartite quantum correlations under power-law and random telegraph noises: collective effects of Markovian and non-Markovian classical fields. *Ann. der Phys.* **534**, 2100584 (2022)
- Reboiro, M., Civitarese, O., Tielas, D.: Use of discrete Wigner functions in the study of decoherence of a system of superconducting flux-qubits. *Phys. Scr.* **90**(7), 074028 (2015)
- Rowe, D.J., Sanders, B.C., De Guise, H.: Representations of the Weyl group and Wigner functions for SU (3). *J. Math. Phys.* **40**(7), 3604–3615 (1999)
- Seyfarth, U., Klimov, A.B., De Guise, H., Leuchs, G., Sánchez-Soto, L.L.: Wigner function for SU (1, 1). *Quantum* **4**, 317 (2020)
- Smith, G., Smolin, J.A., Yard, J.: Quantum communication with Gaussian channels of zero quantum capacity. *Nat. Photonics* **5**(10), 624–627 (2011)
- Sudarshan, E.C.G.: Equivalence of semiclassical and quantum mechanical descriptions of statistical light beams. *Phys. Rev. Lett.* **10**, 277–279 (1963)
- Takagi, S.: Vacuum noise and stress induced by uniform acceleration: Hawking–Unruh effect in Rindler manifold of arbitrary dimension. *Progr. Theor. Phys. Suppl.* **88**, 1–142 (1986)
- Tian, Z., Wang, J., Jing, J.: Nonlocality and entanglement via the Unruh effect. *Ann. Phys.* **332**, 98–109 (2012)
- Unruh, W.G.: Notes on black-hole evaporation. *Phys. Rev. D* **14**, 870 (1976)
- Wigner, E.P.: On the quantum correction for thermodynamic equilibrium. In: Part I: Physical Chemistry, Part II: Solid State Physics, pp. 110–120. Springer (1997)
- Yu, T., Eberly, J.H.: Qubit disentanglement and decoherence via dephasing. *Phys. Rev. B* **68**, 165322 (2003)

Publisher's Note Springer Nature remains neutral with regard to jurisdictional claims in published maps and institutional affiliations.